Inquiro, the UAB undergraduate science research journal

Volume 2012 | Number 6 Article 24

2012

Work Function and HOMO Levels of Zinc Phthalocyanine on Different Substrates

Joseph Olson

Michael Kozlik

Torsten Fritz

Work Function and HOMO Levels of Zinc Phthalocyanine on Different Substrates

Joseph Olson[1], Michael Kozlik[2], Prof. Dr. Torsten Fritz[2]
[1] Department of Mathematics, University of Alabama at Birmingham, Birmingham, AL
[2] Institut für Festkörperphysik, Friedrich-Schiller-Universität, Jena, Germany

Abstract

Ultraviolet photoelectron spectroscopy (UPS) is used to analyze the work function and highest occupied molecular orbital (HOMO) levels of zinc phthalocyanine (ZnPc) as well as the interface between evaporated ZnPc on Au/Si, ZnO/ITO/borosilicate, and AZO/quartz. Also, ultraviolet-visible spectroscopy (UV-Vis) and UPS are used to investigate the heating of ZnPc films at approximately 325°C in order to induce a change from α to β phase. Preliminary to the main investigation, the UPS equipment's bias voltage is calibrated and UPS spectra for Au/Si, ITO/borosilicate, ZnO/ITO/borosilicate, and AZO/quartz are analyzed. While the measured Fermi edges, valence bands, and HOMOs of the samples are in good agreement with previously reported values, the measured work functions are consistently lower than expected. However, the construction of a Au/ZnPc/ZnO/TCO hybrid solar cell, where the TCO is either ITO or AZO, still appears to be feasible.

Introduction

One of the new generations of photovoltaic cells is the "hybrid" solar cell, appropriately named because they are composed of both organic and inorganic materials. There are several benefits of hybrid solar cells. First, they can be mass manufactured at low cost compared to purely inorganic solar cells. Second, they combine the high absorbance of organic materials with the high conductivity of inorganic materials [1]. Third, many organic compounds easily form thin films, allowing a wide array of various layers with different properties to be constructed for specific design [2]. Fig. 1 depicts a general model for a hybrid solar cell. After entering into the solar cell (from the right through a layer of glass not shown in the diagram), light passes through a transparent conducting oxide (TCO) and an inorganic layer before entering an organic layer. In this organic layer, the photons excite an electron from the highest occupied molecular orbital (HOMO) level to the lowest unoccupied molecular orbital (LUMO) level. The HOMO level, as the name indicates, is the energy level of the highest energy electron orbital which contains an electron at ground state while the LUMO level is the energy level of the next highest electron orbital. When an electron is excited to the LUMO level in the organic layer, it becomes available to move within the material, traveling from molecule to molecule. Also, when it becomes excited into the LUMO level, the electron leaves behind a positively charged electron "hole" in the HOMO level. The "hole" travels throughout the material like a positively charged particle, akin to the electron's movement. This electron-hole pair, called an *exciton*, can transfer energy in the material without transferring any net charge. The energy, which originally came from the photon, is stored in the material as a potential difference between the electron and the hole. The binding energy of an exciton in organic materials is on the magnitude of 1 eV, depicted as the energy bumps in the HOMO and LUMO levels in Fig. 1. In the inorganic layer, the conduction band (CB) is analogous to the LUMO level while the valence band (VB) is analogous to the HOMO level. Although the Fermi energy in the metal is analogous to the HOMO level in organic materials, there is one distinct difference: there are always electrons above the Fermi energy in a metal. That is why metals are such excellent conductors. As the excited electrons in the organic layer try to return to ground state, they travel to the inorganic layer since there is a decrease in energy from the LUMO level to the conduction band. Similarly, the holes travel from the organic layer to the metal due to an increase from the HOMO level to the Fermi Energy. This charge separation creates a potential difference and, with the addition of a circuit, a current is produced.

This study uses ultraviolet photoelectron spectroscopy (UPS) to investigate the feasibility of a hybrid solar cell composed of gold as the metal, zinc phthalocyanine (ZnPc) as the organic material, zinc oxide (ZnO) as the inorganic material, and either aluminum-doped zinc oxide (AZO) or tin-doped indium oxide (ITO) as the TCO. The use of phthalocyanine derivatives as organic films in hybrid photovoltaic systems is currently of great interest because of their simple synthesis, thermal stability, and high absorbance [4]. ZnPc is well studied on ITO and C_{60} [4, 5, 6], but to date, little is known about the ZnPc/ZnO interface. ZnO has a high optical transparency in the visible spectral range (ideal for allowing light to pass through to the ZnPc layer) as well as good conductivity on the order of 10^{-3} ohm^{-1} cm^{-1} [7, 8]. AZO and ITO are popular choices as a TCO in optical devices because of their high conductivity and high transparency in the visible spectral range [9, 10]. The work function of a material is the amount of energy needed to remove an electron from that material. AZO was chosen for the front contact because its work function is slightly lower than ITO's work function (which implies the electrons would rather move towards AZO than ITO). Also, AZO is inexpensive to manufacture because of the abundance of aluminum and zinc; the rarity of indium makes ITO more expensive. However, ITO has a critical advantage over AZO. When heated to temperatures exceeding 400°C, AZO on quartz or borosilicate will crack due to a mismatch of thermal expansions. These cracks cause an increase in resistivity [11].

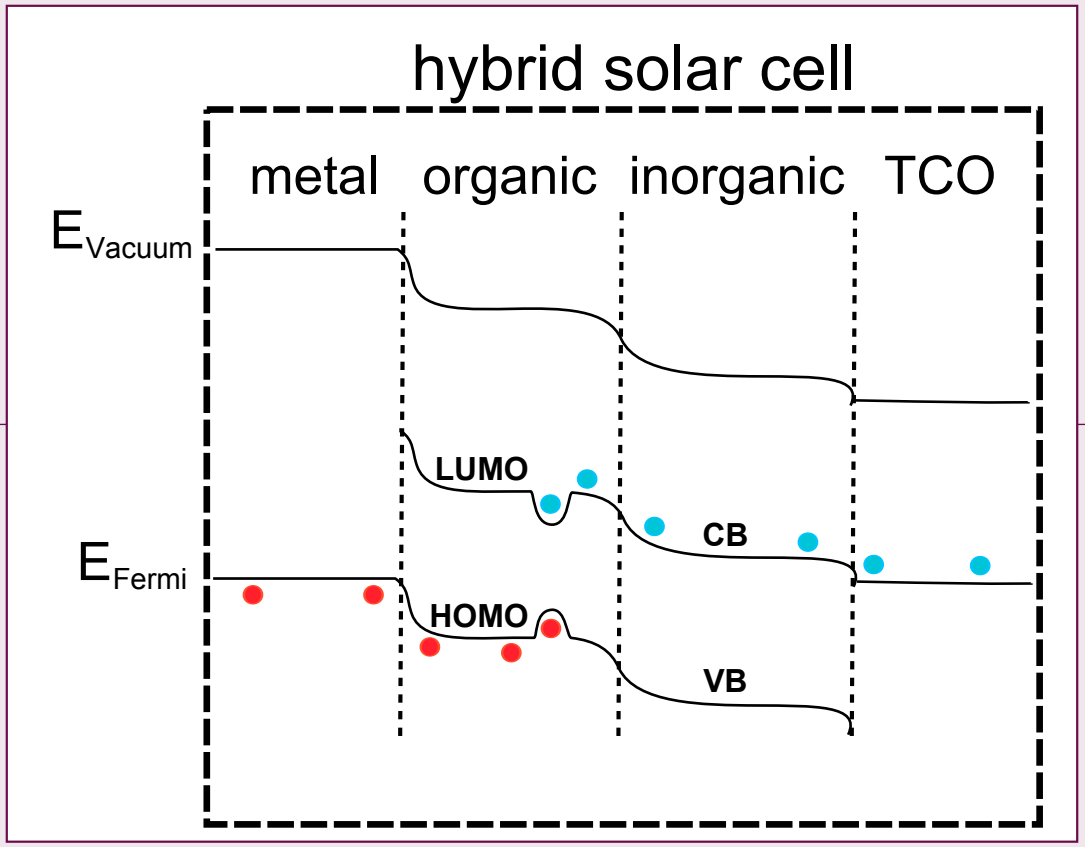

Figure 1. The general schematic of a hybrid solar cell, as described in the first paragraph. Here, the horizontal axis has units of distance indicating the thickness of the different layers of the semiconductor. The vertical axis has units of energy. Electrons are depicted as blue dots while positive holes are depicted as red dots [3].

Such high temperatures are needed to grow ZnO nanowires. Although the addition of ZnO nanowires will not be investigated in this study, ZnO nanowires grown on the ZnO side of the ZnPc/ZnO interface have been shown to significantly enhance conductivity [11].

As ZnPc crystals grow on a surface such as ZnO, they form a series of parallel columns. However, these columns are not directed perpendicular to the surface. In the α phase of ZnPc, the columns are directed at an angle of 25° to the surface normal. In the β phase, the columns are directed at an angle of about 45°-48° to the surface normal. Therefore, the columns of the α phase are closer to being perpendicular to the ZnO surface than the columns of the β phase [12]. The α and β phases have different absorbance spectra in the ultraviolet-visible spectrum range. This is due to the different distances and intermolecular forces acting between neighboring ZnPc molecules in the ZnPc crystal. Ultraviolet-visible spectroscopy (UV-Vis) is used on solid ZnPc crystal films to analyze an α to β phase change due to heating.

UPS uses a discharge lamp, usually helium emitting photons of energy hv = 21.22 eV, to excite electrons in a material. The electrons from the sample material are excited out of the sample and the kinetic energy is measured. The kinetic energy of the electron, KE, depends on the energy of the photon, hv, and the binding energy of the electron, BE, by KE = hv-BE. Furthermore, if a bias voltage, V_{Bias}, is applied, then the spectra undergo a constant horizontal shift. This will appear in the equation as a negative term, yielding KE = hv-BE-V_{Bias} [13]. The area in the spectra of low kinetic energy, or high binding energy (as depicted in Fig. 2) is the secondary electron background which results from electrons losing energy through inelastic scattering before leaving the material [14]. The left most side of the spectra, known as the secondary edge or high binding energy cutoff (HBEC), is where the secondary background ends abruptly [15]. These electrons have just enough energy to make it out of the sample. The work function, W_F, is calculated as the difference W_F = hv-BE_{HBEC} where BE_{HBEC} is the binding energy associated with the high binding energy cutoff [13].

Besides the work function, another important energy is calculated from UPS spectra. If the material is a metal or TCO, this value is the Fermi edge, E_F. If the material is an organic semiconductor, this energy is that of the HOMO level. If the material is an inorganic semiconductor, this value is the valence band maximum, VBM, the highest energy level in the valence band. The Fermi edge, as seen in Fig. 2, is determined by the

low binding energy cutoff (LBEC) on the right side. The LBEC is the sharp cut-off region of the UPS spectra which corresponds to electrons which were measured to have a low binding energy. These are electrons at the surface which escape with a large kinetic energy. Since a semiconductor has non-metallic layers, a semiconductor's spectra will not have a visible Fermi edge but will instead have a peak of minimum binding energy, corresponding to the HOMO level or the valence band. Due to the relatively low energy used, UPS measures only the valence levels (outer electron orbitals) of a material, not the core levels. UPS measurements are very sensitive to the surface of the material due to the limited *mean free path* of electrons in this energy range - the average distance traveled by an electron before colliding with another particle. Thus, electrons emitted from the material during UPS measurements can only originate from areas close to the surface [13].

Materials and Methods

Preparation

Sputtering is the process in which a material is decomposed by the bombardment of high energy particles (such as argon). Thin films may be made by collecting the atoms ejected from this material on some surface. Multiple 100 nm gold films on silicon were prepared by sputtering. Each one was sputtered with pure argon gas at a pressure of 8 Pa and at a rate of 1 nm/s. The gold was exposed to air while being transferred to the UPS chamber. Several 400 nm AZO films were also sputtered on quartz. AZO was sputtered with pure argon gas with a flow of 6 sccm (standard cubic centimeter per minute) at a pressure of 10^{-3} mbar. The concentration of aluminum doping is 2% by mass. The AZO films were exposed to air while being transferred to the UPS chamber. ZnO films were likewise sputtered onto ITO/borosilicate with a flow of 6 sccm at a pressure of 10^{-3} mbar. It was sputtered with a mixed gas of argon and 2 atm% oxygen. Both 100 nm and 200 nm ZnO films were prepared. The ZnO samples also were exposed to air while being transferred to the UPS chamber.

ZnPc films were prepared in a B30 high vacuum evaporation chamber (Oerlikon Leybold Vacuum Dresden GmbH, Germany). The chamber pressure before evaporation varied slightly for each film, ranging from 2×10^{-5} mbar to 5×10^{-5} mbar. The chamber pressure during evaporation ranged from 2×10^{-5} mbar to 20×10^{-5} mbar. Most commonly, the evaporation pressure was about 5×10^{-5} mbar. Also, the rate of evaporation varied from 0.3 Å/s to 1.0 Å/s (1 Å = 10^{-10} m) and the temperature at which evaporation began was between 260°C and 280°C. ZnPc films of varying thickness ranging from 1 nm to 100 nm were evaporated on both 100 nm ZnO/ITO/borosilicate and 400 nm AZO/quartz. ZnPc/ZnO will be used to mean ZnPc on 100

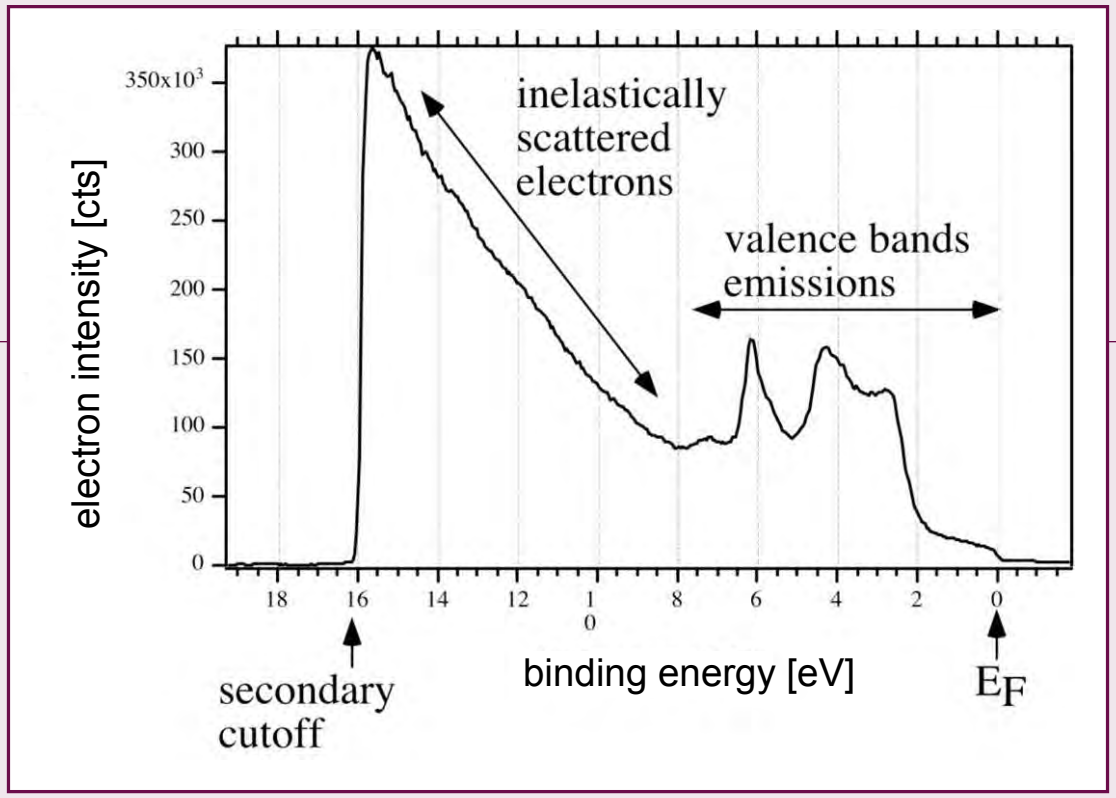

Figure 2. UPS spectra of gold (Au) [15]

nm ZnO/ITO/borosilicate and ZnPc/AZO will be used to mean ZnPc on 400 nm AZO/quartz. An oscillating quartz was used to measure film thickness. The measurements were calibrated by measuring the thickness of a 100 nm copper film on silicon with surface profiler Dektak 3030 (Veeco/Sloan, United States). The oscillating quartz was then used to determine the thickness of the ZnPc films by using the density parameter of ZnPc, 1.62 g/cm^3.

After performing UPS measurements on all the ZnPc films, some samples were heated and measured again in order to investigate a phase change in ZnPc. Prior to heating, 10 nm ZnPc/AZO and 10 nm ZnPc/ZnO were analyzed in UV-Vis. Then they were heated on a hot plate in an open environment to 350° ± 10°C for 10 min. The heated 10 nm ZnPc films were first measured in the UV-Vis then transferred directly to the UPS for analysis. Also, 50 nm ZnPc/AZO and 50 nm ZnPc/ZnO were measured with UV-Vis then heated on the same hot plate at 325° ± 10°C for 10 min. The heated 50 nm ZnPc films were first measured in the UPS then transferred to the UV-Vis spectrometer for analysis.

Methods and Calculation

The samples were analyzed in the UPS with He(I) (hv=21.22 eV) and He(II) (hv=40.8 eV) excitation [16]. The range of energy analyzed was from 4 eV to 50 eV for all unheated 10 nm and 50 nm ZnPc films, ZnO/ITO/borosilicate, ITO/borosilicate, and AZO/quartz samples, as well as all the Au/Si samples used to calibrate the bias voltage. For the heated 10 nm and 50 nm ZnPc films and the unheated 1, 2, 3, and 5 nm ZnPc films, the range of the energy analyzed was from 8 eV to 54 eV. The range of energy analyzed changed so that, with a -9 V bias voltage, the He(II) Fermi Edge of the samples, which was shifted from 40.8 eV to roughly 50 eV, would still be clearly visible. The pressure in the UPS chamber varied between 1.7 x 10^{-7} and 2.2 x 10^{-7} mbar. The UPS data is actually measured in intensity per channel instead of intensity per binding, energy so a correlation between the channels and binding energy needs to be established. Also, the applied bias voltage for that measurement needs to be considered. The appropriate relationship to use is BE = hv-KE-V_{Bias}. The He(I) and He(II) Fermi edges of gold spectra are well documented, so these values were used to generate a linear correspondence of the 1,508 channels used in the UPS measurements to binding energy for the energy axis.

The Fermi edge was determined by the same method Olthof used in her dissertation [13]. The value taken for the Fermi edge was the point of intersection between a linear approximation for the low binding energy cutoff and a linear approximation for the baseline as shown in Fig. 2. This method was also used in determining the $HOMO_{onset}$ and valence band maximum. As depicted in Fig. 4, the $HOMO_{onset}$ is the highest energy level of the HOMO energy band while $HOMO_{max}$ is the most common energy level of the HOMO energy band. The high binding energy cutoff was determined by calculating half of the intensity of the secondary electron background peak and finding the corresponding binding energy as done by Yoshitake [17]. Fig. 2 depicts this method schematically. The work function is then calculated by W_F = hv-BE_{HBEC}.

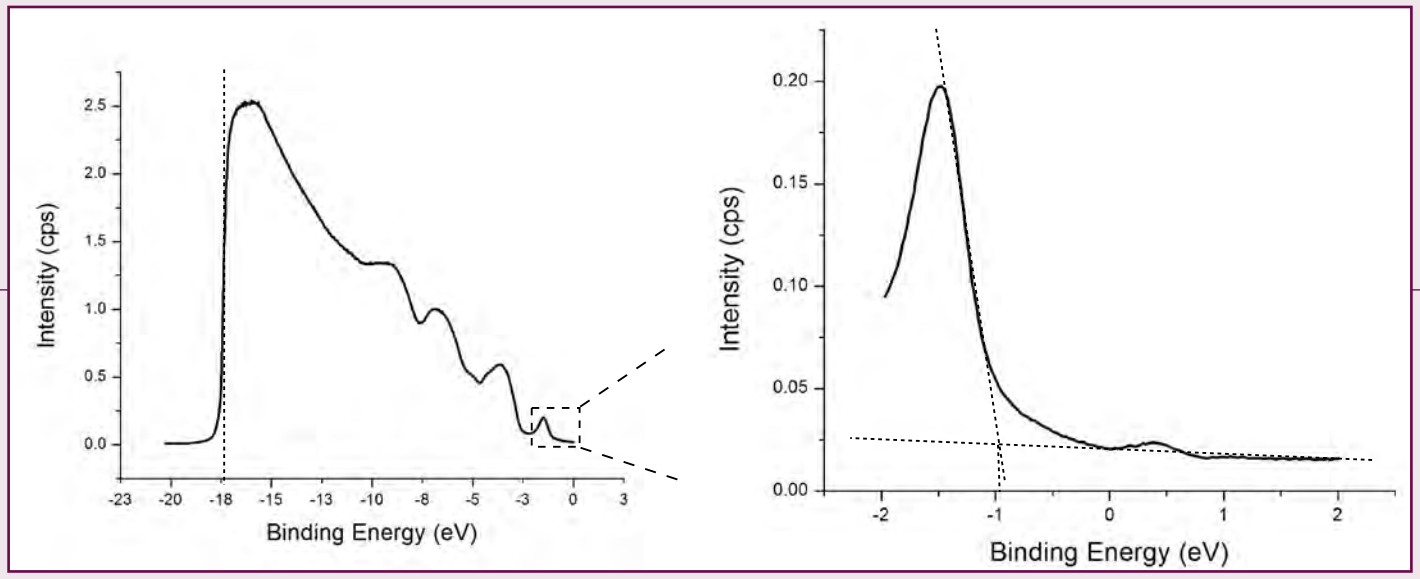

Figure 3. UPS spectra for 10 nm ZnPc/AZO. The HBEC (left) is determined to be the binding energy corresponding to half of the intensity of the secondary electron background peak. The HOMOonset (right) is determined to be the point of intersection between a linear approximation for the low binding energy cutoff and a linear approximation for the baseline.

Results and Discussion

The HOMO and valence band levels of the samples are in good agreement with previously found values in the literature. However, the work function of the samples is consistently lower than expected. The measured work function of the gold samples ranges from 4.17 eV to 4.52 eV with an average of 4.36 eV. According to literature, the work function of gold is between 4.8 eV and 5.2 eV [18, 19]. Considering the value 3.09 eV as an outlier, the measured work function of ZnO ranges from 3.35 eV to 3.53 eV with an average of 3.47 eV. The work function for ZnO on silicon cited in literature is 4.3 eV to 4.5 eV [8]. The average valence band maximum is measured to be 3.14 eV which is close to other reported values of 3.15 eV to 3.25 eV [20, 21]. Thus it seems the right side of the UPS spectra is accurate while the left side is inaccurate. Information could be lost in the bulk peak of the secondary electron background.

Sample Thickness (nm)	$HOMO_{onset}$ (eV)	$HOMO_{max}$ (eV)	Work Function (eV)
1	n/a	n/a	4.03
2	n/a	n/a	4.05
3	n/a	n/a	4.06
5	-0.62	-1.23	4.31
10	-0.79	-1.29	4.55

Table 1. Optical measurements of various ZnPc films on a gold substrate.

Sample Thickness (nm)	$HOMO_{onset}$ (eV)	$HOMO_{max}$ (eV)	Work Function (eV)
1	-1.17	-1.75	3.80
2	-0.93	-1.51	3.62
3	n/a	n/a	3.94
5	-0.90	-1.47	3.70
10	-1.05	-1.48	3.84
50	-1.17	-1.72	3.75

Table 2. Optical measurements of various ZnPc films on an AZO substrate.

Sample Thickness (nm)	$HOMO_{onset}$ (eV)	$HOMO_{max}$ (eV)	Work Function (eV)
1	n/a	n/a	3.59
2	-0.96	-1.57	3.65
3	-1.01	-1.66	3.68
5	-0.91	-1.57	3.87
10	-0.97	-1.45	3.98
50	n/a	n/a	3.37

Table 3. Optical measurements of various ZnPc films on a ZnO substrate.

AZO was measured to have a work function of 3.71 eV. Since the work function of AZO is strongly dependent on the level of aluminum doping and the O/Zn ratio [10], values have been reported as low as 3.7 eV and as high as 4.5 eV [10, 22]. It is generally found that a higher mass % of Al relates to a higher work function. The highest reported mass% of Al is 1.35% which is lower than the measured 2% in this study. The work function found by Jiang et al. corresponding to AZO with mass % of Al at 1.35% is 4.4 eV, which is much higher than the measured work function of 3.71 eV in this study [10]. The O/Zn ratio of the measured AZO sample is unknown.

The average work function of the two measured ITO samples is 3.75 eV. Literature values of ITO's work function range from 4.1 eV to 5.5 eV, with 4.6 eV and 4.7 eV being the most commonly cited values [23, 24, 25]. The large gap in reported values could be due to the particularly high sensitivity of the ITO surface to the environment.

In general, the low work functions could be due to water, oxygen, or other contaminants on the surfaces. This is likely since the samples were exposed to air while transferring them to the UPS and film surfaces can be very sensitive to environmental exposure. A sputter chamber and surface profiler inside the UPS would resolve this issue since the samples would be able to be prepared and analyzed without leaving a vacuum.

No literature was found containing the work function, $HOMO_{onset}$, or $HOMO_{max}$ of ZnPc on ZnO, AZO, or gold. However, ZnPc on ITO is reported to have a work function of 4.14 ± 0.1 eV, $HOMO_{onset}$ at -1.04 ± 0.05 eV, and $HOMO_{max}$ at -1.49 ± 0.05 eV [4].

As shown in Table 1, the $HOMO_{onset}$ and $HOMO_{max}$ are not visible for 1, 2, and 3 nm ZnPc films on gold. This is probably due to an incomplete or very thin layer of ZnPc. The work function of ZnPc increased with film thickness. Although the measured work functions are generally low, the relation between the measured work function of ZnPc on gold and the measured work function of gold is interesting. At first, ZnPc lowers the work function of pure gold, but as the layer becomes thicker, the work function actually surpasses gold's. The work functions of ZnPc films on gold are found to be similar to the work functions found of ZnPc films on ITO. Both HOMO levels of the 5 and 10 nm ZnPc films are lower than those of ZnPc on ITO.

As indicated in Table 2, all ZnPc on AZO films, except the 3 nm film, have a visible $HOMO_{onset}$ and $HOMO_{max}$. There is no correlation between the sample thickness and the $HOMO_{onset}$, $HOMO_{max}$ or work function. However, the ZnPc on AZO HOMO levels are not only higher than those of ZnPc on gold, they are also in good agreement with those of ZnPc on ITO. The work functions, however, are lower than those of ZnPc on gold and the reported values of ZnPc on ITO.

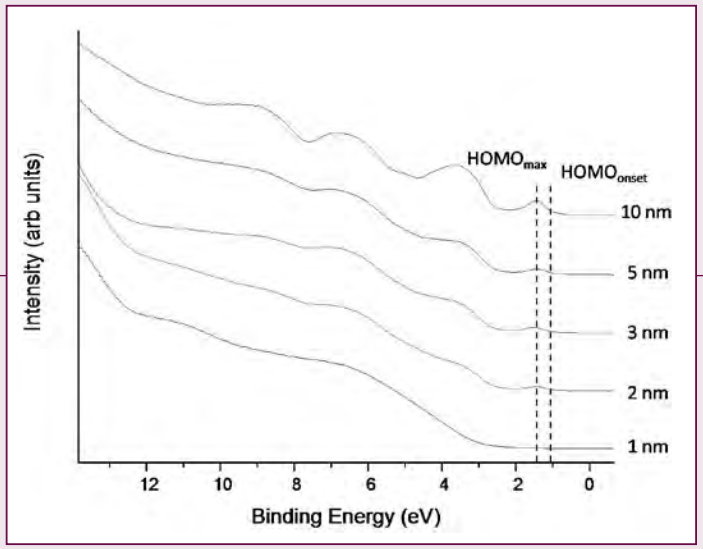

Figure 4. UPS spectra for various films of ZnPc on 100 nm ZnO. HOMOonset corresponds to the point at which the molecular orbital is first visible while HOMOmax corresponds to the peak.

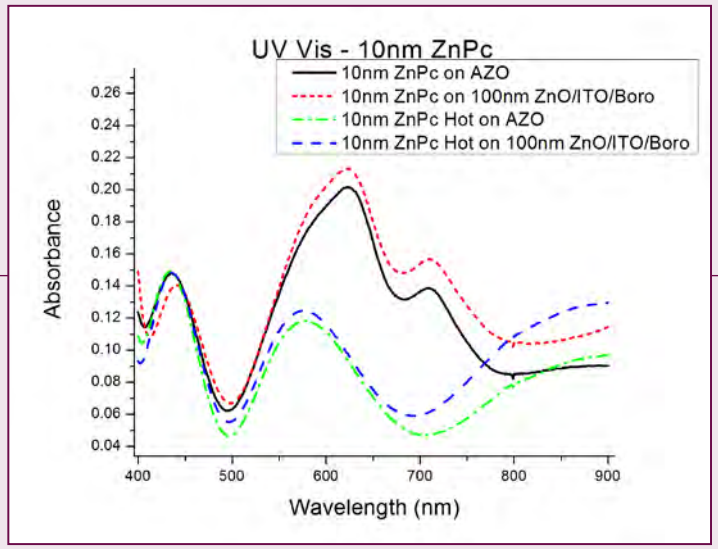

Figure 5. UV-Vis spectra of 10 nm ZnPc samples before and after heating.

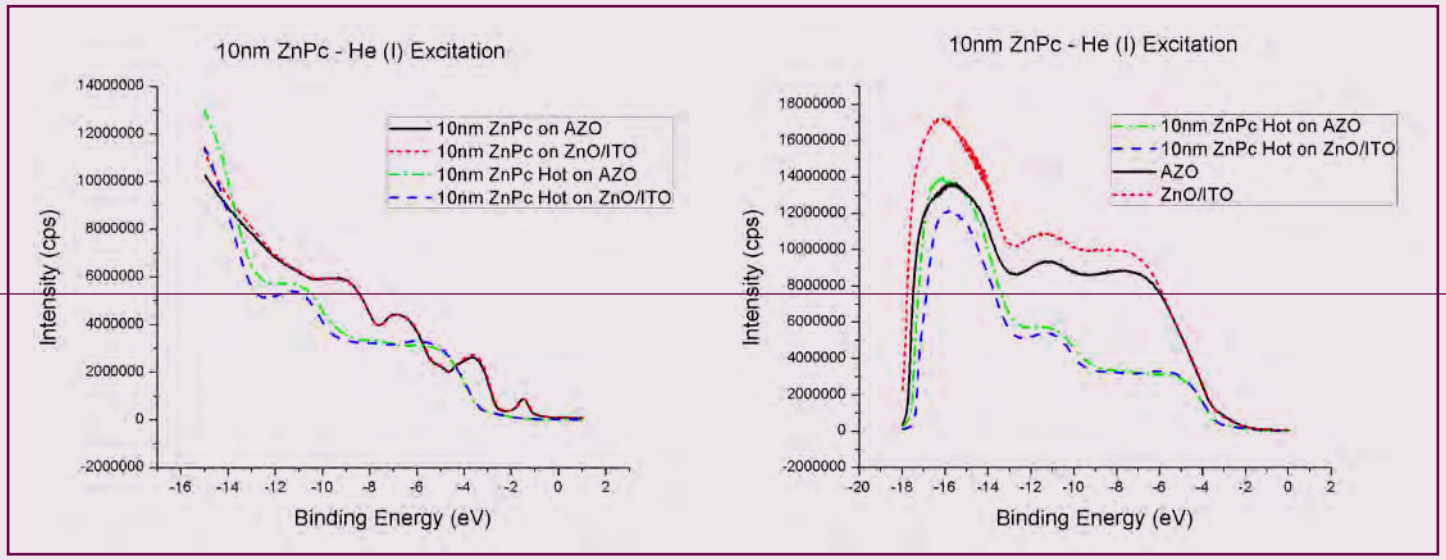

Figure 6. On left, UPS spectra of 10 nm ZnPc samples before and after heating. On right, UPS spectra of heated 10 nm ZnPc samples compared to UPS spectra of the samples' substrates.

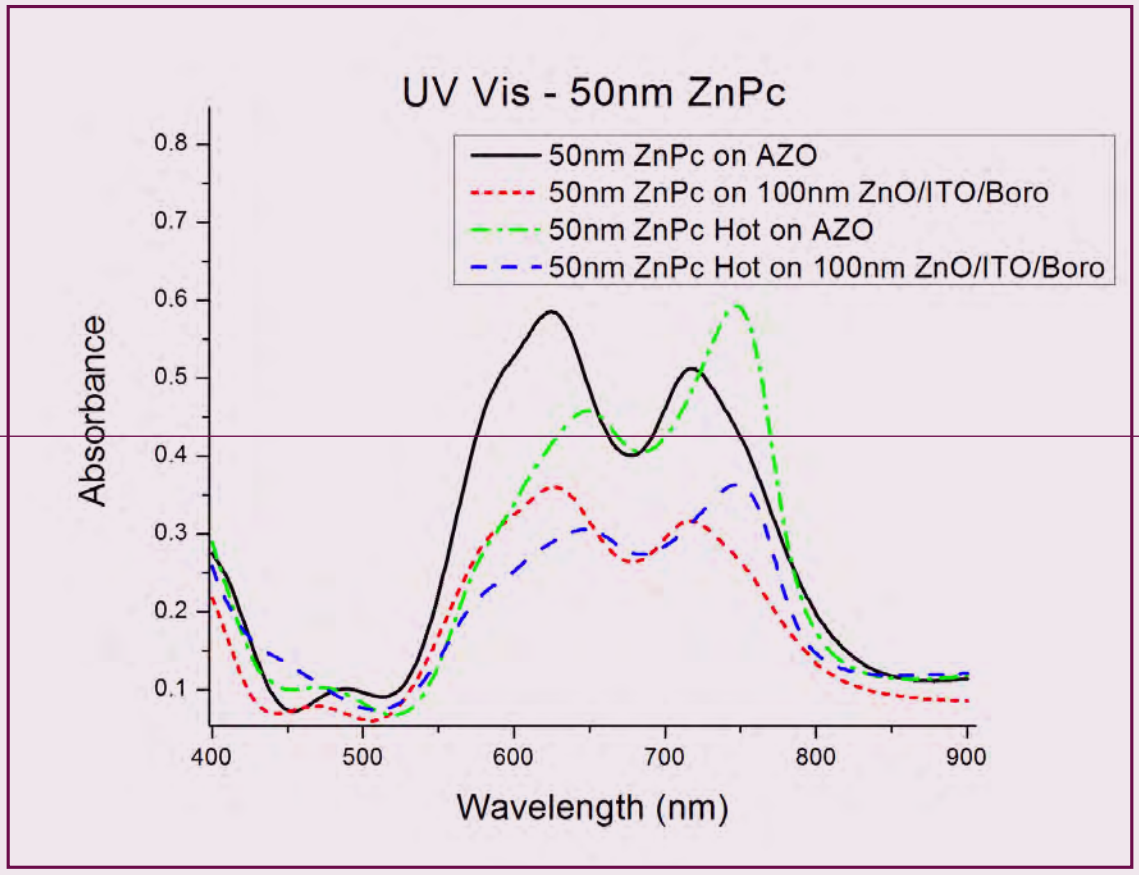

Figure 7. UV-Vis spectra of 50 nm ZnPc samples before and after heating.

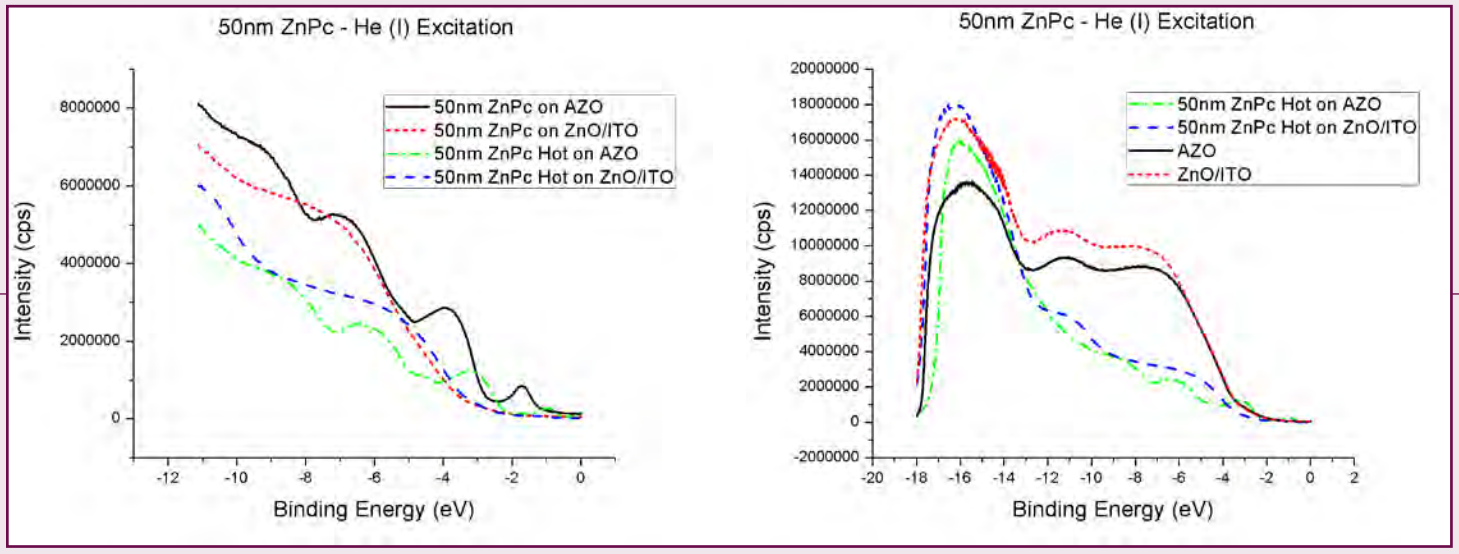

Figure 8. On left, UPS spectra of 50 nm ZnPc samples before and after heating. On right, UPS spectra of heated 50 nm ZnPc samples compared to UPS spectra of the samples' substrates.

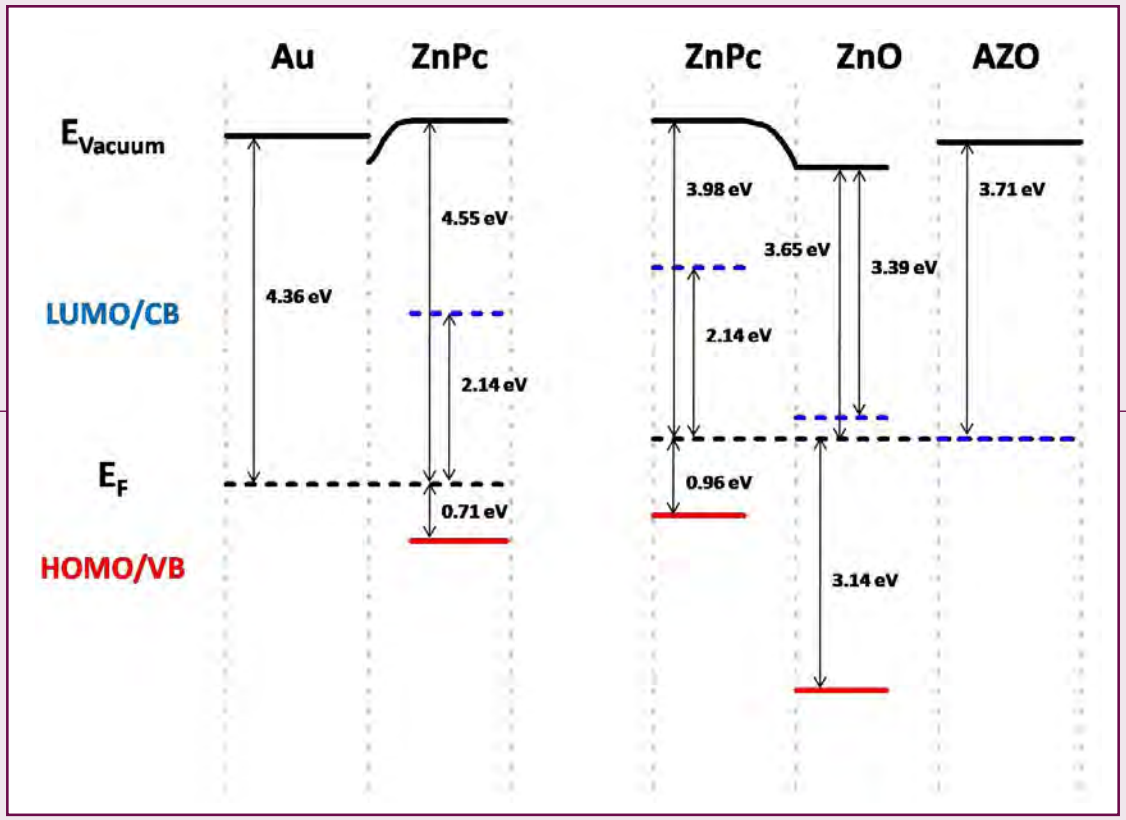

Figure 9. Band diagram of a solar cell constructed of gold, ZnPc, ZnO and AZO. Blue lines correspond to the lowest unoccupied molecular orbital levels and the red lines correspond to the highest occupied molecular orbital levels and the valence band.

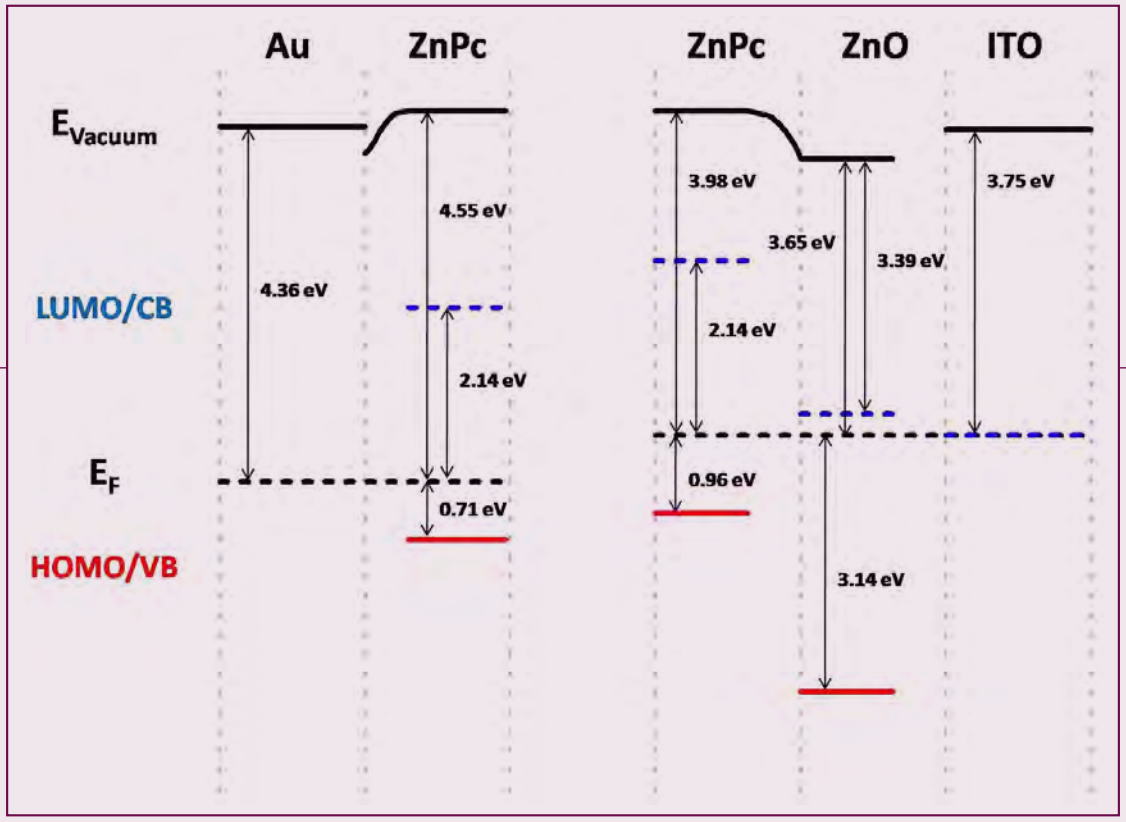

Figure 10. Band diagram of a solar cell constructed of gold, ZnPc, ZnO and ITO. Blue lines correspond to the lowest unoccupied molecular orbital levels and the red lines correspond to the highest occupied molecular orbital levels and the valence band.

Fig. 4 shows the UPS spectra of various ZnPc films on ZnO while Table 3 shows the numerical values of the measured optical properties. It is clear from the diagram that the HOMO levels are not visible until 2 nm of thickness. As the thickness of the ZnPc layer increases, the HOMO levels become more pronounced and the work function increases from that of ZnO to 3.98 eV.. The work function of ZnPc on ZnO is generally close to that of ZnPc on AZO. Both $HOMO_{onset}$ and $HOMO_{max}$ are seemingly unrelated to film thickness, but are in good agreement with the HOMO levels found of ZnPc on ITO.

The α and β phases of ZnPc are investigated by heating ZnPc samples on a hot plate in the open air. It is found that the evaporation chamber evaporates ZnPc in the α phase which can be converted to the β phase upon heating. The α and β phases of ZnPc have characteristic UV-Vis peaks. The α phase has an absorbance peak around 630 nm which has a higher intensity than another peak around 700 nm [26]. However, the β phase has a peak around 650 nm which has a lower intensity than the other peak around 750 nm [27]. Both 10 nm ZnPc on AZO and 10 nm ZnPc on ZnO exhibit an α phase before heating as seen in Fig. 5. However, after heating at 350° ± 10°C for 10 min, the peak around 700 nm simply vanishes in both spectra. Furthermore, the UPS spectra of the heated 10 nm ZnPc on AZO and 10 nm ZnPc on ZnO resemble the spectra of their respective substrates. The graph on the left of Fig. 6 shows that the UPS spectra of the heated ZnPc looks quite different from that of the non-heated ZnPc. The graph on the right of Fig. 6 shows that heated ZnPc samples resemble the UPS spectra for that of their respective substrates. This is likely due to interference effects since the films in these samples are relatively thin.

Fig. 7 shows that both 50 nm ZnPc on AZO and 50 nm AZO on ZnO exhibit α phase UV-Vis spectra before heating. After heating at 325° ± 10°C for 10 min, the UV-Vis spectra of these samples resemble the β phase. This supports the previous claim that the 10 nm ZnPc films did not exhibit a phase change because they were relatively thin compared to the 50 nm ZnPc films. Evidence for this explanation is also supported by the UPS spectra on the right side of Fig. 8. Here, the spectra of heated ZnPc films do not resemble to UPS spectra of their respective substrates. The UPS spectra in the left graph of Fig. 8 show a shift in HOMO level of ZnPc on AZO before and after heating. The $HOMO_{onset}$ before heating is -1.17 eV but after heating is -0.52 eV. The $HOMO_{max}$ before heating is -1.72 eV but after heating is -1.08 eV. The reason for the HOMO shift is unknown. Since the HOMO level of both the heated and unheated ZnPc is higher in energy than the valence band of ZnO, either the α or β phase will work in this hybrid solar cell design. However, the α phase has higher conductivity which makes it more desirable [26].

Conclusion

Figures 9 and 10 show band diagrams for solar cells composed of gold, ZnPc, ZnO, and either AZO or ITO, respectively. Although, ZnPc on ZnO/AZO is not a sample that was investigated, it is included in a separate band diagram because AZO and ITO show similar energy cutoffs in their individual UPS spectra. In fact, the only difference between the two band diagrams, besides the change in labeling from AZO to ITO, is a change in the TCO work function from 3.71 eV to 3.75 eV. Because of the two different work functions measured for bulk ZnPc, one of ZnPc on gold and the other of ZnPc on ZnO, the band diagrams are split into two halves. It is believed that the work function between the two differ by 0.57 eV because of a change in Fermi edge due to different substrates. This is depicted in the diagrams by aligning the vacuum energy and shifting the Fermi energy. However, it could also be due to surface contamination. Since the HOMO levels have no correlation with film thickness like the work function does, the HOMO levels in the band diagrams are determined by the average of the $HOMO_{onset}$ measurements. The LUMO and conduction bands are predicted by using band gap values taken from literature. These values are assumed in the band diagrams.

The band diagrams indicate that the solar set-up is feasible. The diagrams show a decreasing energy level from the ZnPc LUMO level, to the ZnO conduction band, to the TCO (AZO or ITO) Fermi edge. As depicted in the general hyrbid solar cell schematic, Fig. 1, this allows for the excited electron to move from the organic layer to the TCO. Also, the increase in energy from the ZnPc HOMO level to gold's Fermi edge allows for the hole to move towards the metal. Since the valence band of ZnO is lower in energy than the HOMO level on ZnPc, the hole is kept from moving towards the TCO.

However, more investigation needs to be done before precise conclusions can be made. Primarily, the reason for the work functions being consistently lower than expected needs to be investigated further. Since *in situ* UPS experiments are impossible to perform with the available equipment, it is difficult to resolve whether or not it is due to surface contamination. If the problem persists, perhaps a low temperature scanning tunneling microscope could be used to confidently determine any correlation between levels of surface contamination and differences in work function. Also, it should be established whether AZO or ITO is best to use for the TCO. It may be that a combination of the two, ZnO/AZO/ITO, is the best option. Although it would not be the cheapest design, the ITO may prevent the AZO from cracking while the AZO would provide a low work function contact with ZnO.

References

1. S. Günes, N. S. Sariciftci. Hybrid Solar Cells. *Inorg. Chim. Acta* 361 (2008), 581-588.

2. E. Arici, N. S. Sariciftci, D. Meissner. Hybrid solar cells. *Encyclopedia of Nanoscience and Nonotechnology* 3, 929- 944.

3. This graphic was provided by Michael Kozlik.

4. Y. Gassenbauer, A. Klei. Electronic and chemical properties of tin-doped indium oxide (ITO) surfaces and ITO/ZnPc interfaces studied in-situ by photoelectron spectroscopy. *J. Phys. Chem. B* 110 (2006), 4793-4801.

5. C. Hein, E. Mankel, T. Mayer, W. Jaegermann. Engineering the electronic structure of the ZnPc/C60 heterojunction by temperature treatment. *Solar Energy Materials & Solar Cells* 94 (2010), 662-667.

6. S. H. Park et. al. The electronic structure of C60 /ZnPc interface for organic photovoltaic device with blended layer architecture. *Appl. Phys. Lett.* 96 (2010), 013302.

7. R. B. Lal, G. M. Arnett. Effect of Ultra-violet irradiation on the electrical conductivity of zinc oxide single crystals. *Nature* (1965), no. 5017, 1305.

8. K. B. Sundaram, A. Khan. Work function determination of zinc oxide films. *J. Vac. Sci. Technol. A* 15 (1997), no. 2, 428- 430.

9. H. Zhou et. al. Preparation of aluminum doped zinc oxide films and the study of their mircostructure, electrical and optical properties. *Thin Solid Films* 515 (2007), 6909-6914.

10. X. Jiang, F. L. Wong, M. K. Fung, S. T. Lee. Aluminum-doped zinc oxide films as transparent conductive electrode for organic light-emitting devices. *Appl. Phys. Lett.* 83 (2003), no. 9, 1875-1877.

11. S. Möller, Wachstum. von senkrechten ZnO-Nanodrähten auf verschiedenen Glassubstraten. *Institut für Festkörperphysik auf Friedrich-Schiller-Universität Jena* (2010).

12. F. Iwatsu. Size effects on the α-β Transformation of Phthalocyanine Crystals. *J. Phys. Chem.* 92 (1988), 1678- 1681.

13. S. S. Olthof. Photoelectron spectroscopy on doped organic semiconductors and related interfaces. Dissertation, Technische UniversitÃ¤t Dresden (2010).

14. R. Schlaf. Calibration of photoemission spectra and work function determination. Dept. of Electrical Engineering at the University of South Florida. Retrieved from http://rsl.eng.usf.edu/ Documents/Tutorials/PEScalibration.pdf. June 08, 2011

15. R. Schlaf. Tutorial on Work Function. Dept. of Electrical Engineering at the University of South Florida. Retrieved from http://rsl. eng.usf.edu/Documents/Tutorials/TutorialsWorkFunction.pdf. June 08, 2011

16. D. Comdei, A. R. Zanatta, F. Alvarez, I. Chambouleyron, Photoelectron spectroscopy of shallow core levels using HeII (40.8) excitation. *J. Vac. Sci. Technol. A* 13 (1995), no. 4, 2278-2280.

17. M. Yoshitake. Principle and practical tips of work function measurement using UPS, XPS, and AES instruments. *Hyomen Kagaku* 28 (2007), no. 7, 397-401.

18. P. A. Anderson. Work function of gold. *Phys. Rev.* 115 (1959), no. 3, 553-554.

19. W. N. Hansen, K. B. Johnson. Work function measurements in gas ambient. *Surf. Sci.* 316 (1994), 373- 382.

20. B Carlson, K. Leschkies, E. S. Aydil, X. Y. Zhu. Valence band alignment at cadmium selenide quantum dot and zinc oxide interfaces. *J. Phys. Chem.* C 112 (2008), 8419-8423.

21. K. Sawada, Y. Shirotori, K. Ozawa, K. Edamoto, M. Nakatake. Valence band structure of the ZnO surface studied by angle-resolved photoemission spectroscopy. *Appl. Surf. Sci.* 237 (2004), 343-347.

22. K. Schulze et. al. Organic solar cells on indium tin oxide and aluminum doped zinc oxide anodes. *Appl. Phys. Lett.* 91 (2007), 073521.

23. F. Nesch, L. J. Rothberg, E. W. Forsythe, Q. T. Le, Y. Gao. A photoelectron spectroscopy study of the indium tin oxide treatment by acids and bases. *Appl. Phys. Lett.* 74 (1999), no. 6, 880-882.

24. Y. Park, V. Choong, Y. Gao, B. R. Hsieh, C. W. Tang. Work function of indium tin oxide transparent conductor measured by photoelectron spectroscopy. *Appl. Phys. Lett.* 68 (1996), no. 19, 2699-2701.

25. S. W. Tong, K. M. Lau, H. Y. Sun, M. K. Fung, C. S. Lee, Y. Lifshitz, S. T. Lee. Ultraviolet photoelectron spectroscopy investigation of interface formation in an indium-tin oxide/fluorocarbon/organic semiconductor contact. *Appl. Surf. Sci.* 252 (2006), 3806-3811.

26. M. Kozlik, S. Paulke, M. Gruenewald, R. Forker, T. Fritz. Determination of the optical constants of α and β zinc (II) phthalocyanine films. *Organic Electronics* (2012) accepted.

27. L. Gaffo, M. R. Cordeiro, A. R. Freitas, W. C. Moreira, E. M. Girotto, V. Zucolotto. The effects of temperature on the molecular orientation of zinc phthalocyanine films. *J. Mater. Sci.* 45 (2010), 1366-1370.

Special thanks to Prof. Dr. Torsten Fritz, Michael Kozlik, and the FSU Festkörperphysik department for their hospitality.

Authors' Addresses

Joseph Olson
Department of Mathematics, University of Alabama at Birmingham, Birmingham, AL 35294-1170
jwolson@uab.edu

Michael Kozlik
Institut für Festkörperphysik, Friedrich-Schiller-Universität, Jena, Germany 07743
michael.kozlik@uni-jena.de

Prof. Dr. Torsten Fritz
Institut für Festkörperphysik, Friedrich-Schiller-Universität, Jena, Germany 07743
torsten.fritz@uni-jena.de